ARTICLE

Photocatalytic Activity Improvement of g-C_3N_4 under Visible Light by Optimizing Preparation Conditions

Jian-yang Hu[a*], Guo-li Zhu[b]

a. School of Chemistry & Materials Science, University of Science and Technology of China, Hefei 230026, China
b. Dalian Institute of Chemical Physics, Chinese Academy of Sciences, Dalian 116023, China

(Dated: Received on June 9, 2015; Accepted on September 21, 2015)

Graphite-like C_3N_4 (g-C_3N_4) is an efficient visible-light-driven photocatalyst which is commonly used in pollutant degradation. The photoreactivity of g-C_3N_4 depends on the preparation conditions to a large extent. In this work, we linked the preparation conditions of g-C_3N_4 to its stability and photocatalytic activity through dye photodegradation experiments and sensitivity mathematical analyses. The sensitivity mathematical analyses show that the effect of calcination temperature is more significant than calcination time on the photoreactivity of g-C_3N_4. The photocatalytic activity of optimized g-C_3N_4 in rhodamine B (RhB) degradation under visible light was 100 times higher than that of non-optimized one. The enhanced performance can be attributed to the increased specific surface area of g-C_3N_4 and the increased migration velocity of photogenerated electron-hole pairs on the surface. This work deepens the understanding of the relation between preparation conditions and the charateristics of g-C_3N_4, and provides an extremely simple method for significantly improving the photoreactivity of g-C_3N_4.

Key words: g-C_3N_4, Photocatalysis, Preparation condition, Optimization, Sensitivity analysis

I. INTRODUCTION

Photocatalytic technology using metal oxide semiconductors has attracted much attention as one of the energy-efficient techniques in wastewater treatment and surface water remediation [1−3]. However, most metal oxide photocatalysts release toxic metal ions and can only utilize UV light to generate conduction band electrons (e^-) and valence band holes (h^+) for contaminant reduction [4−6]. Graphitic carbon nitride (g-C_3N_4), which consists only of carbon and nitrogen, has been applied to different photocatalytic fields [7−11] under visible light to minimize environmental risk and increase the efficiency of solar utilization. This polymeric semiconductor is environment friendly, highly stable, inexpensive, and presents intrinsic visible light response [12, 13].

Despite its advantages, g-C_3N_4 exhibits low photoreactive efficiency because of the high recombination rate of its photogenerated charges [14]. Thus, most studies currently focused on the modification of pure g-C_3N_4, such as fabrication of a porous structure [15, 16], doping with metal or nonmetal elements [17, 18], coupling with graphene [19], and combining with other semiconductors [20, 21]. Although these methods obviously improve g-C_3N_4 photocatalytic activity, the complex preparation process, high cost, and biological toxicity of the resultant photocatalysts reveal the need for further studies. Changing preparation conditions to influence the photoreactivity and stability of g-C_3N_4 is an extremely simple modification method. For example, Dong *et al.* [22] found the specific surface area and crystallinity of g-C_3N_4 increased with increasing heating temperatures, leading to improvement of photocatalytic activity. Yan *et al.* [9] observed the C/N ratio increased and the band gap decreased with increasing preparation temperature of g-C_3N_4. Despite most studies on the calcination temperature in the preparation of g-C_3N_4, another important preparation parameter, calcination time, has usually been disregarded. Systematical elucidation of the effects of preparation conditions on photoreactivity of g-C_3N_4 is necessary.

In the present study, we investigated the effects of both temperature and calcination time on the photoreactivity of g-C_3N_4 and proposed an optimized preparation method to significantly improve the photoreactivity of g-C_3N_4. g-C_3N_4 samples were prepared by changing both calcined temperature and calcination time, the preparation parameters were optimized by decolorization experiments of rhodamine B (RhB) and significance analysis method, the physico-chemical properties

*Author to whom correspondence should be addressed. E-mail: hjychina@mail.ustc.edu.cn, Tel.: +86-551-63607482

of g-C_3N_4 samples were analysized by a series of characterizations, and the underlying mechanism of preparation conditions influencing the photocatalytic activity of g-C_3N_4 was also investigated.

II. MATERIALS AND METHODS

The g-C_3N_4 photocatalyst was prepared by directly heating melamine in a semiclosed system to prevent melamine sublimation. Then, 10 g of melamine powder was placed in an alumina crucible with a cover and then heated to 450, 500, 550, or 600 °C in a muffle furnace for 2, 4, or 8 h at a heating rate of 4.17 °C/min. The resultant yellow powder was collected and used without further treatment.

Powder X-ray diffraction (XRD) patterns (2θ=10°−70°) were obtained on an MXPAHF X-ray diffractometer (MaxScience, Japan) operated at 18 kV and 450 mA with Cu Kα radiation (λ=1.54056 Å). The morphologies of g-C_3N_4 were observed on a SIRION 200 scanning electron microscope (FEI, USA) operated at an accelerating voltage of 5 kV. The UV-Vis diffuse reflection spectra (DRS) of dry-pressed disk samples were obtained using a SOLID 3700 spectrophotometer (Shimadzu Inc., Japan) equipped with an integrating sphere assembly; here, $BaSO_4$ was used as the reference. X-ray photoelectron spectra (XPS) were obtained on an ESCALAB 250 X-ray photoelectron spectroscopy system (Thermo Fisher, USA) with Al Kα radiation ($h\nu$=1486.6 eV) as the excitation source. The binding energies were calibrated by referencing the C1s peak (284.6 eV) to reduce the sample charge effect. The texture properties of g-C_3N_4 were observed on a TRISTAR II 3020 specific surface area and pore size analyzer (Micromeritics, USA).

Photocatalytic degradation of RhB was performed in a 125 mL magnetically stirred cylindrical reactor top-irradiated by a 350 W Xenon lamp (XD-300, Nanjing Yanan Special Lighting Co., Ltd.) at room temperature (26 °C). In a typical run, 80 mL of 10 mg/L RhB aqueous solution was added to the reactor. The pH of the RhB solution was adjusted to a set value of 7 using 1 mol/L $HClO_4$ and NaOH solutions. A 150 mg portion of the photocatalyst was added to the reactor, and the system was stirred in the dark for 30 min to achieve adsorption equilibrium. This degradation process is similar to that described in our previous work [23]. The samples were centrifuged to sediment the photocatalyst, and the RhB concentration in the supernatants was monitored by measuring solution absorbance using a UV-2450 spectrophotometer (Shimadzu Inc., Japan) at 553.5 nm wavelength. Based on the approach above, we conducted a photocatalytic decolorization experiment of RhB using different g-C_3N_4 samples prepared under various conditions. Each experiment was tested at least in triplicate.

IBM SPSS software (Version 21) was used to analyze the significance of the factors influencing the properties of g-C_3N_4. Double-factor variance analysis without considering interactions was suitably used as the significance analysis method.

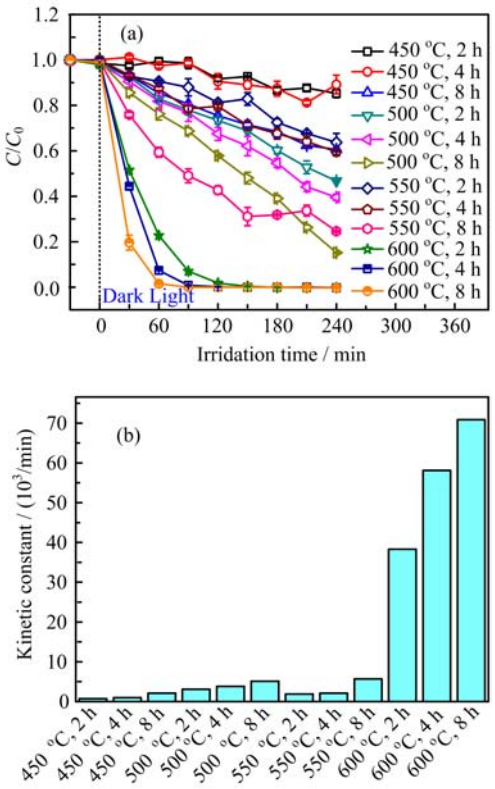

FIG. 1 (a) Adsorption property and (b) photocatalytic activities of g-C_3N_4 samples synthesized by heating melamine at different temperatures and durations for degradation of RhB under visible light.

III. RESULTS AND DISCUSSION

A. Optimization of preparation conditions

The photocatalytic degradation of RhB experiments were conducted to evaluate the effects of calcination temperature and calcination time on the photoreactivity of g-C_3N_4. The curves of degradation RhB by g-C_3N_4 samples are shown in Fig.1(a). RhB is confirmed to be stable under visible light thus its self-degradation process can be ignored [24]. Under the catalytic effect of g-C_3N_4, RhB is gradually degraded with the extension of illumination time, in which the degradation efficiency is gradiently enhanced along with the increasement of calcination temperature and calcination time. A significant improvement of RhB degradation appeares when using g-C_3N_4 prepared at 600 °C as the photocatalyst. The removal ratio of RhB reaches more than 99% after the irradiation of 150 min. The photocatalytic degradation process accords with the pseudo first-order kinetics

DOI:10.1063/1674-0068/29/cjcp1505123

TABLE I Influencing factors for significant analysis of the photocatalytic properties of g-C_3N_4 with dependent variable of %.

Source	Type III sum of squares	df	Mean square	F	p (Sig.)
Corrected model	13440.839[a]	5	2688.168	60.732	4.7×10^{-5}
Intercept	13881.386	1	13881.386	313.614	2.0×10^{-6}
Calcination temperature	12737.125	3	4245.708	95.921	1.8×10^{-5}
Calcination time	703.714	2	351.857	7.949	2.1×10^{-2}
Error	265.576	6	44.263		
Total	27587.800	12			
Corrected total	13706.415	11			

[a] R^2=0.981 (adjusted R^2=0.964).

TABLE II Influencing factors for significant analysis of the crystallographic parameters of g-C_3N_4 with dependent variable of (°).

Source	Type III sum of squares	df	Mean square	F	p(Sig.)
Corrected model	0.319	5	0.064	49.412	8.5×10^{-5}
Intercept	9185.333	1	9185.333	7111225.806	0.0
Calcination temperature	0.305	3	0.102	78.658	3.3×10^{-5}
Calcination time	0.014	2	0.007	5.542	4.3×10^{-2}
Error	0.008	6	0.001		
Total	9185.660	12			
Corrected Total	0.327	11			

[a] R^2=0.981 (adjusted R^2=0.964).

(Eq.(1)) by data fitting, thus the apparent kinetic constant (k_{app}) can be used to compare the photocatalytic activity of each g-C_3N_4 sample quantitatively [25, 26]:

$$\ln(C/C_0) = k_{app}t \quad (1)$$

From Fig.1(b), k_{app} increases with the increase of calcined temperature and calcination time. The maximum k_{app} of all g-C_3N_4 samples is 7.09×10^{-2} min^{-1} (600 °C, 8 h), which is more than 100-fold higher than the minimum k_{app} of 7×10^{-4} min^{-1} (450 °C, 2 h). This suggests that the preparation conditions indeed influence the photocatalytic activity of g-C_3N_4 significantly. Similar results have been reported in Refs.[27, 28]. However, this factor has dominant impact on the photoreactivity of g-C_3N_4 is still unclear.

To evaluate the effects of calcination temperature and calcination time on the photodegradation of RhB, the significance analysis was adopted by calling the "univariate" process of the data statistics software IBM SPSS (Version 21) to examine the differences of various influencing factors. The significance of factors influencing g-C_3N_4 photoreactivity was analyzed, and results are listed in Table I. The p-values of calcination temperature and calcination time are lower than 0.05, which indicates that these factors significantly affect g-C_3N_4 photoreactivity. However, the p-value of calcination temperature is remarkably smaller than that of calcination time, which means calcination temperature is the primary sensitive factor affecting g-C_3N_4 photoreactivity [29].

B. Characterization

To verify the effects of calcination temperature and calcination time on the crystallographic parameters of g-C_3N_4, 12 groups of XRD patterns were taken (Fig.S1 in supplementary materials), and the significance analysis was adopted again. The consequence was consistent with the sensitivity analysis results before (shown in Table II), the calcination temperature evidently influences the crystal structure of g-C_3N_4 rather than the calcination time. In this work, we choose the g-C_3N_4 samples prepared with a relative long time (8 h) at 450, 500, 550, and 600 °C (denoted CN-450, CN-500, CN-550, and CN-600, respectively) to characterize, thus to reveal the underlying relation between the calcination temperature and photoreacticity of g-C_3N_4.

1. XRD to characterize the crystallographic parameters

The XRD patterns and the crystallographic parameters of the g-C_3N_4 samples are shown in Fig.2(a) and Table III, respectively. Two peaks at 2θ of approximately 27.7° and 13.1° are found in all samples. The

DOI:10.1063/1674-0068/29/cjcp1505123

TABLE III The crystallographic parameters of g-C_3N_4 samples synthesized at different temperatures.

Catalyst	d_{100}/nm	d_{002}/nm	FWHM$_{002}$/(°)	2θ/(°)	Mean crystallite size/nm
CN-450	0.663	0.324	0.950	27.52	8.61
CN-500	0.669	0.323	0.830	27.61	9.86
CN-550	0.673	0.321	0.742	27.72	11.0
CN-600	0.685	0.319	0.572	27.96	14.3

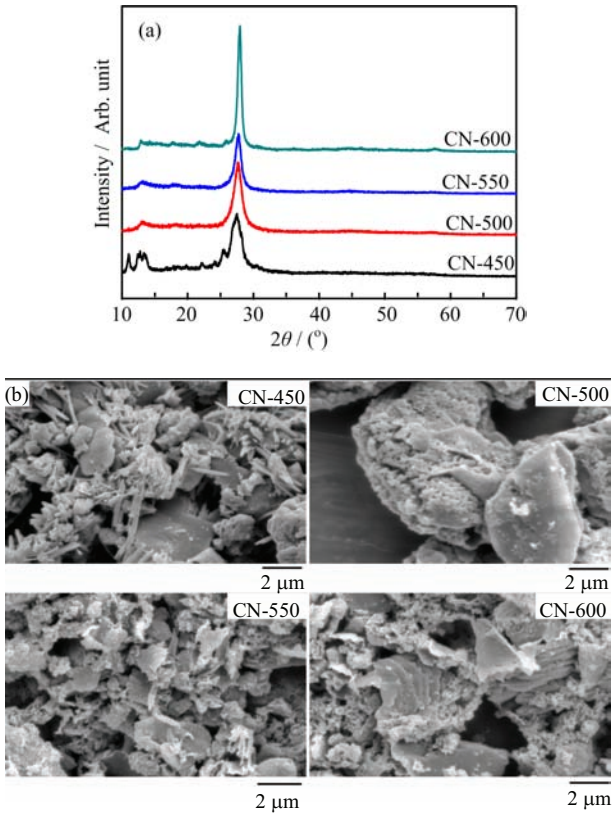

FIG. 2 (a) XRD patterns and (b) SEM images for g-C_3N_4 samples synthesized by heating melamine at different temperatures for 8 h.

peak at 27.7° reveals the typical interlayer-stacking (002) of extended conjugated aromatic segments, and the peak at 13.1° represents in-plane packing of tri-*s*-triazine units (100), which are based on tri-*s*-triazine building blocks [30]. The (002) peak shifts toward higher diffraction angles from CN-450 at 27.52° to CN-600 at 27.96° as the temperature increases. The interlayer distance of the 100 crystal plane (d100) decreases from 0.324 nm to 0.319 nm whereas the interlayer distance of the 002 crystal plane (d002) increases from 0.663 nm to 0.685 nm as the temperature increases from 450 °C to 600 °C. The mean crystallite size of g-C_3N_4 calculated using the Scherrer formula [31] significantly increases from 8.61 nm to 14.3 nm with temperature, which means high temperatures can promote crystal growth or aggregation and tend to form larger grains. This phenomenon suggests that the crystal structure of g-C_3N_4 obtained at high temperature are more stable than that obtained at low temperature [9, 22]. Other peaks corresponding to the crystalline melamine ($C_3H_6N_6$) phase are detected in CN-450.

2. SEM to characterize the surface morphology

To determine the surface morphology of g-C_3N_4 under different preparation conditions, the SEM images of all g-C_3N_4 samples were taken and the results are obviously different between each other (shown in Fig.2(b)). Samples treated by low temperatures (CN-450 and CN-500) are composed of compact particles with irregular shapes and sizes. The acicular structure in the SEM image of CN-450 may be attributed to the melamine residual. In contrast, the morphology of samples is more ordered and dominantly comprises aggregated layers with a size of several micrometers after raising temperatures even further (CN-550 and CN-600). The reason why the morphology evolves from granular to layer is that the process of thermal condensation is promoted by the increasing temperature, thus the condensation degree is increased, which causes the growth of the laminated structure [27].

3. UV-Vis DRS to characterize the optical absorption property

In order to measure the optical absorption property and energy band position of materials, the UV-Vis DRS of all g-C_3N_4 samples are shown in Fig.3(a). The absorption edges of all of the samples at ∼450 nm show strong visible light absorption. As the temperature increases from 450 °C to 600 °C, the absorption edge initially shifts up and then slightly decreases. The band gap energy (E_g) was estimated from the intercept of the tangents to the curves of $[F(R_\infty)h\nu]^{1/2}$ versus photon energy ($h\nu - E_g$) by Kubelka-Munk transformation (Fig.3(b)) [32]. The calculated E_g value is approximately 2.7 eV, which is consistent with earlier studies [33]. Compared with the band gap energies of other catalysts, CN-500 exhibits a smaller E_g of 2.67 eV, implying that CN-500 has broader optical responses; on the other hand, CN-600 exhibits a larger E_g of 2.92 eV, revealing that CN-600 has higher electrode potential, stronger redox ability of photongenerated carrier, and better photocatalytic activities than the other photocatalysts studied.

DOI:10.1063/1674-0068/29/cjcp1505123

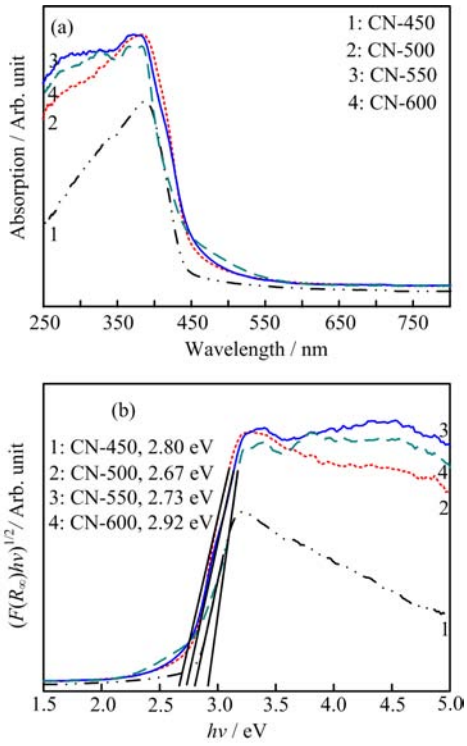

FIG. 3 (a) UV-Vis DRS and (b) plots of $(\alpha h\nu)^{1/2}$ *vs.* photon energy of g-C_3N_4 samples synthesized by heating melamine at different temperatures for 8 h.

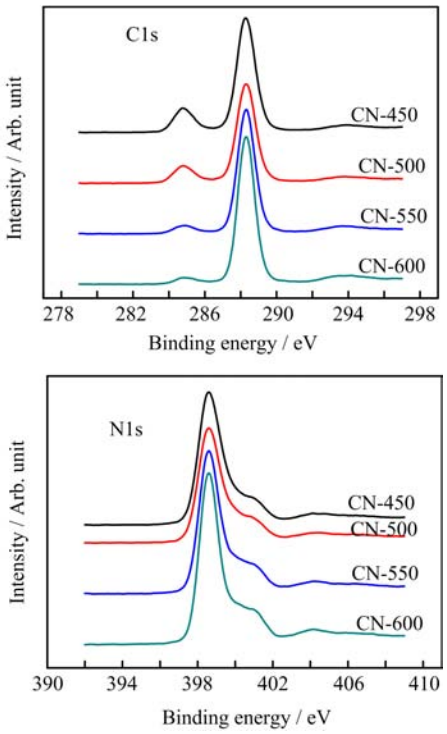

FIG. 4 XPS patterns for g-C_3N_4 samples synthesized by heating melamine at different temperatures for 8 h.

TABLE IV The surface element contents of g-C_3N_4 samples synthesized at different temperatures.

Catalyst	C/%	N/%	O/%	C/N ratio
CN-450	42.43	56.25	1.32	0.754
CN-500	42.58	55.98	1.44	0.761
CN-550	42.9	56.21	0.89	0.763
CN-600	42.85	56.48	0.68	0.759

4. XPS to characterize the oxidation state and surface chemical composition

XPS spectra were obtained to analyze the oxidation state and surface chemical composition of the g-C_3N_4 photocatalysts. The XPS spectra of C1s and N1s for all g-C_3N_4 samples are shown in Fig.4. In Fig.4(a), the C1s peak at 284.8 eV, which corresponds to C−C coordination, is due to carbon-containing contaminations; the C1s peak at 288.3 eV is related to N−C−N coordination in the graphitic carbon nitride [34, 35]. As calcination temperature increases, the peak at 284.8 eV weakens from CN-450 to CN-600 because of decreases in the crystalline melamine ($C_3H_6N_6$) phase. This phenomenon illustrates the improved purity and photocatalytic activity of g-C_3N_4. The N1s peak at 398.6 eV, another characteristic peak of g-C_3N_4, is displayed in Fig.4(b), this peak could be ascribed to C−N−C coordination in the graphitic carbon nitride [36]. The C/N ratios calculated by XPS are list in Table IV, and all ratios are near 0.75, an standard atom ratio of g-C_3N_4. Compared with other samples, CN-550 exhibited the highest C/N ratio of 0.763, which indicates that the remarkably increased photocatalytic activity may be due to more complete condensation in the sample [37]. Improvements in the photocatalytic properties of CN-600 compared with those of CN-550 may be attributed to higher heating temperatures resulting in decreases in structural integrity in the final product and increases in lattice defects [38].

5. BET to characterize the texture properties

As the most general preparation condition in g-C_3N_4 studies, the physico-chemical properties of CN-550 are closer to CN-600 than other g-C_3N_4 samples. Therefore, we further analyze the texture properties of CN-550 and CN-600 by BET (Table V) to explore the influence of calcination temperatures on the physico-chemical properties of g-C_3N_4. The specific surface area and pore volume of CN-600 is 34.4 m^2/g and 0.117 cm^3/g, which are about 2.7- and 2.4-fold larger than CN-550, respectively. The phenomenon shows that the increase of calcination temperature does lead to changes of the catalyst morphology; the wider surface area and more pore structure of CN-600 are consistent with the characterization aforementioned as well.

DOI:10.1063/1674-0068/29/cjcp1505123

TABLE V The texture properties of g-C_3N_4 samples synthesized at different temperatures.

Catalyst	S_{BET}[a]/(m^2/g)	V_p[b]/(cm^3/g)	d[c]/nm
CN-550	12.7	0.049	26.7
CN-600	34.4	0.117	24.9

[a] Calculated by Brunauer-Emmett-Teller (BET) model.
[b] Pore volume was calculated at P/P_0=0.97.
[c] Average pore diameter was calculated by adsorption isotherm using BJH method.

In addition, since the stacked layer structure is formed in CN-600 compared to the irregular compact particles of samples treated by low temperatures, the surface-to-volume ratio of CN-600 also increases to a certain extent.

C. Mechanism

Generally, photocatalysts are excited by photons to produce conduction band electrons (e^-) and valence band holes (h^+). The redox reactions in the photocatalytic process can be induced only when photogenerated electron-hole pairs migrate to the surface of photocatalysts. Therefore, with the enlargement of the specific surface area of materials, these redox reactions can obtain more active sites (reaction sites), thus directly improve the photocatalytic activity. Amano *et al.* [39] proved the good linear relation between photocatalytic activity and specific surface area of one photocatalyst in the premise of keeping other physico-chemical properties unchanged as far as possible. In this work, the specific surface area of g-C_3N_4 increases from 12.7 m^2/g to 34.4 m^2/g, which directly enhance the photocatalytic activity. However, the growth speed of photocatalytic activity is faster than that of surface area: we calculate the intrinsic photoreactivity (k_S) of materials by normalizing surface area (S_{BET}) with apparent kinetic constant (k_{app}) (Eq.(2)). k_S value of CN-550 and CN-600 is 0.45 and 2.06 mg/(min·m^2), respectively.

$$k_S = \frac{k_{app}}{S_{BET}} \tag{2}$$

The results clearly show that increased calcination temperature contributes to enhancing the intrinsic photoreactivity. Viewed from another perspective, preparation conditions may cause other physico-chemical properties change besides specific surface area to promote the photocatalytic activity of g-C_3N_4, which need to be further discussed and confirmed.

As we know, intrinsic photoreactivity of a photocatalyst is mainly influenced by three processes: (i) excitation process after photons absorption, (ii) migration and composite process of electron-hole pairs on the surface, (iii) redox reaction process induced by electron-hole pairs on the surface. As the intrinsic photoreactivity is not affected by specific surface area according to Eq.(2), process (iii) is mainly determined by the potential of electron-hole pairs. However, the band position of g-C_3N_4, which is calculated by Mott-Schottky electrochemical method [40−42], does not change significantly after preparation conditions were optimized [18, 43]. So we basically consider that preparation conditions will not affect process (iii). Moreover, the band gap of g-C_3N_4 increases from 2.67 eV (CN-500) to 2.92 eV (CN-600) with the calcination temperature increase, which leads to reducing visible light availability of g-C_3N_4 and inhibiting the occurrence of process (i), but this phenomenon is contrary to the fact of elevated intrinsic photoreactivity of g-C_3N_4 synthesized at higher temperature. Therefore, we postulate that preparation conditions mainly revise process (ii) to raise the intrinsic photoreactivity of g-C_3N_4. It means that longer life expectancy and lower recombination rate of photogenerated charges is another critical element to promote photocatalytic activity besides specific surface area.

IV. CONCLUSION

Compared with well-known photocatalysts that can only utilize UV light, g-C_3N_4 is one of the few non-doped photocatalysts that use visible light, which is its unique advantage. We optimize the preparation conditions of g-C_3N_4 and successfully improve its stability and visible light photocatalytic activity. The dye photodegradation experiments and sensitivity mathematical analyses can quickly determine the main factors affecting the photocatalytic activity, thus improving the preparation efficiency of g-C_3N_4. Our study shows that both calcination temperature and calcination time have a significant influence on the photocatalytic activity of g-C_3N_4, but the former is more sensitive. The photocatalytic activity of g-C_3N_4 after optimization of preparation conditions in the degradation of RhB under visible light was more than 100 times of non-optimized g-C_3N_4, which was attributed to the increased SSA of the material and also the increased migration velocity of photogenerated electron-hole pairs.

Supplementary materials: Twelve groups of XRD patterns were taken in supplementary materials so as to verify the effects of calcination temperature and calcination time on the crystallographic parameters of g-C_3N_4 convincingly.

[1] J. Zhao, C. Chen, and W. Ma, Top. Catal. **35**, 269 (2005).
[2] M. R. Hoffmann, S. T. Martin, W. Choi, and D. W. Bahnemann, Chem. Rev. **95**, 69 (1995).
[3] H. Gnayem and Y. Sasson, ACS Catal. **3**, 186 (2013).
[4] L. Ma-Hock, S. Brill, W. Wohlleben, P. M. A. Farias, C. R. Chaves, D. P. L. A. Tenrio, A. Fontes, B. S. Santos,

DOI:10.1063/1674-0068/29/cjcp1505123

R. Landsiedel, V. Strauss, S. Treumann, and B. van Ravenzwaay, Toxicol. Lett. **208**, 115 (2012).
[5] M. Li, S. Pokhrel, X. Jin, L. Mädler, R. Damoiseaux, and E. M. V. Hoek, Environ. Sci. Technol. **45**, 755 (2011).
[6] I. K. Konstantinou and T. A. Albanis, Appl. Catal. B **49**, 1 (2004).
[7] K. Maeda, J. Phys. Chem. C **113**, 4940 (2009).
[8] G. H. Dong and L. Z. Zhang, J. Mater. Chem. **22**, 1160 (2012).
[9] S. Yan, Z. Li, and Z. Zou, Langmuir **25**, 10397 (2009).
[10] L. Ge, C. Han, and J. Liu, Appl. Catal. B **108**, 100 (2011).
[11] S. C. Lee, H. O. Lintang, and L. Yuliati, Chem. Asian J. **7**, 2139 (2012).
[12] Y. Wang, X. Wang, and M. Antonietti, Angew. Chem. Int. Ed. **51**, 68 (2012).
[13] Y. Zheng, J. Liu, J. Liang, M. Jaroniecc, and S. Qiao, Energy Environ. Sci. **5**, 6717 (2012).
[14] Y. Zhang, T. Mori, J. Ye, and M. Antonietti, J. Am. Chem. Soc. **132**, 6294 (2010).
[15] X. Wang, K. Maeda, X. Chen, K. Takanabe, K. Domen, Y. Hou, X. Fu, and M. Antonietti, J. Am. Chem. Soc. **131**, 1680 (2009).
[16] H. Yan, Chem. Commun. **48**, 3430 (2012).
[17] X. Wang, X. Chen, A. Thomas, X. Fu, and M. Antonietti, Adv. Mater. **21**, 1609 (2009).
[18] G. Liu, P. Niu, C. Sun, S. C. Smith, Z. Chen, G. Lu, and H. Cheng, J. Am. Chem. Soc. **132**, 11642 (2010).
[19] Q. Xiang, J. Yu, and M. Jaroniec, J. Phys. Chem. C **115**, 7355 (2011).
[20] H. Yan and H. Yang, J. Alloys Compd. **509**, 26 (2011).
[21] X. Xu, G. Liu, C. Randorn, and J. T. S. Irvine, Int. J. Hydrogen Energ. **36**, 13501 (2011).
[22] F. Dong, L. Wu, Y. Sun, M. Fu, Z. Wu, and S. C. Lee, J. Mater. Chem. **21**, 15171 (2011).
[23] X. Zhang, J. Hu, and H. Jiang, Chem. Eng. J. **256**, 230 (2014).
[24] R. W. Ramette and E. B. Sandell, J. Am. Chem. Soc. **78**, 4872 (1956).
[25] S. C. Yan, Z. S. Li, and Z. G. Zou, Langmuir **26**, 3894 (2010).
[26] G. Dong, K. Zhao, and L. Zhang, Chem. Commun. **48**, 6178 (2012).
[27] Y. Zhang, Q. Pan, G. Chai, M. Liang, G. Dong, Q. Zhang, and J. Qiu, Sci. Rep. **3**, 1 (2013).
[28] X. Li, J. Zhang, L. Shen, Y. Ma, W. Lei, Q. Cui, and G. Zou, Appl. Phys. A **94**, 387 (2009).
[29] R. Nuzzo, Nature **506**, 150 (2014).
[30] A. Thomas, A. Fischer, F. Goettmann, M. Antonietti, J. Muller, R. Schlogl, and J. M. Carlsson, J. Mater. Chem. **18**, 4893 (2008).
[31] N. C. Castillo, A. Heel, T. Graule, and C. Pulgarin, Appl. Catal. B **95**, 335 (2010).
[32] F. Dong, S. Guo, H. Wang, X. Li, and Z. Wu, J. Phys. Chem. C **115**, 13285 (2011).
[33] X. Wang, K. Maeda, A. Thomas, K. Takanabe, G. Xin, J. M. Carlsson, K. Domen, and M. Antonietti, Nat. Mater. **8**, 76 (2009).
[34] Y. Zhang, J. Liu, G. Wu, and W. Chen, Nanoscale **4**, 5300 (2012).
[35] L. Ge and C. Han, Appl. Catal. B **117**, 268 (2012).
[36] W. Lei, D. Portehault, R. Dimova, and M. Antonietti, J. Am. Chem. Soc. **133**, 7121 (2011).
[37] P. Niu, L. Zhang, G. Liu, and H. M. Cheng, Adv. Funct. Mater. **22**, 4763 (2012).
[38] K. Hideki and A. Kudo, J. Phys. Chem. B **106**, 5029 (2002).
[39] F. Cardon and W. P. Gomes, J. Phys. D **11**, 63 (1978).
[40] K. Gelderman, L. Lee, and S. W. Donne, J. Chem. Educ. **84**, 685 (2007).
[41] F. Amano, K. Nogami, M. Tanaka, and B. Ohtani, Langmuir **26**, 7174 (2010).
[42] C. Baumanis and D. W. Bahnemann, J. Phys. Chem. C **112**, 19097 (2008).
[43] J. Wang, P. Guo, M. Dou, Y. Cheng, P. G. Jönsson, and Z. Zhao, RSC Adv. **4**, 51008 (2014).

DOI:10.1063/1674-0068/29/cjcp1505123